

Received 17 March 2023, accepted 12 April 2023, date of publication 24 April 2023, date of current version 1 May 2023.

Digital Object Identifier 10.1109/ACCESS.2023.3269694



RESEARCH ARTICLE

An Interpretable Skin Cancer Classification Using Optimized Convolutional Neural Network for a Smart Healthcare System

**KRISHNA MRIDHA¹, (Member, IEEE), MD. MEZBAH UDDIN¹,
JUNGPIL SHIN², (Senior Member, IEEE), SUSAN KHADKA¹,
AND M. F. MRIDHA³, (Senior Member, IEEE)**

¹Department of Computer Engineering, Marwadi University, Rajkot, Gujarat 360003, India

²Department of Computer Science and Engineering, University of Aizu, Aizuwakamatsu 965-8580, Japan

³Department of Computer Science, American International University-Bangladesh, Dhaka 1229, Bangladesh

Corresponding author: Jungpil Shin (jpshin@u-aizu.ac.jp)

This work was supported by JSPS KAKENHI Grant Number JP23H03477.

ABSTRACT Skin cancer is a prevalent form of malignancy globally, and its early and accurate diagnosis is critical for patient survival. Clinical evaluation of skin lesions is essential, but it faces challenges such as long waiting times and subjective interpretations. Deep learning techniques have been developed to tackle these challenges and assist dermatologists in making more accurate diagnoses. Prompt treatment of skin cancer is vital to prevent its progression and potentially life-threatening consequences. The use of deep learning algorithms can improve the speed and accuracy of diagnosis, leading to earlier detection and treatment. Additionally, it can reduce the workload for healthcare professionals, allowing them to concentrate on more complex cases. The goal of this study was to develop reliable deep learning (DL) prediction models for skin cancer classification; (i) deal with a typical severe class imbalance problem, which arises because the skin-affected patients' class is significantly smaller than the healthy class; and (ii) interpret the model output to better understand the decision-making mechanism (iii) Propose an End-to-End smart healthcare system through an android application. In a comparison examination with six well-known classifiers, the effectiveness of the proposed DL technique was explored in terms of metrics relating to both generalization capability and classification accuracy. A study used the HAM10000 dataset and an optimized CNN to identify the seven forms of skin cancer. The model was trained using two optimization functions (Adam and RMSprop) and three activation functions (Relu, Swish, and Tanh). Furthermore, an XAI-based skin lesion classification system was developed, incorporating Grad-CAM and Grad-CAM++ to explain the model's decisions. This system can help doctors make informed skin cancer diagnoses in their early stages, with an 82% classification accuracy and 0.47% loss accuracy.

INDEX TERMS Skin cancer, explainable AI, CNN, Grad-CAM, Grad-CAM++.

I. INTRODUCTION

The World Health Organization has announced skin cancer is a rising global concern, accounting for 33.33% of all cancer cases (WHO) [1]. Over the last decade, the incidence rate has grown dramatically in nations such as the United States, Australia, and Canada. Each year, over 15,000 individuals are

The associate editor coordinating the review of this manuscript and approving it for publication was Mingbo Zhao¹.

killed by skin cancer [2]. In 2021, 7180 individuals died from just one type of skin cancer in the United States, and 7650 people are expected to die from melanoma cancer in 2022 [3]. The amount of hazardous ultraviolet (UV) radiation is being increased due to the depletion of the Ozone layer and it is reaching the earth's surface, causing skin cell damage and raising the risk of skin cancer [4]. Smoking, alcohol intake, certain disorders, infections, and the environment are all variables that contribute to the creation of malignant cells. Skin

tumors are classified as either malignant or non-malignant. Malignant tumors are malignant and exist in a variety of shapes [5].

Skin cancer has increased significantly in the United States, Australia, and Canada during the previous decade [6]. Skin cancer kills an estimated 15,000 individuals each year [7]. According to an American study, 7180 individuals died from just one type of skin cancer in 2021, and 7650 people are expected to die from melanoma cancer in 2022 [8]. Malignant cutaneous adnexa, fibrous histiocytomas, Kaposi's sarcoma, and pleomorphic sarcoma are all examples of skin cancer. The ozone layer's depletion increases the quantity of dangerous ultraviolet (UV) radiation that is reaching the Earth's surface. UV radiation can cause skin cell damage and the growth of malignant cells. This hazardous UV radiation can have a variety of deleterious consequences, including an increase in the risk of skin cancer [9]. Smoking, alcohol intake, numerous disorders, infections, and the living environment are all elements that lead to the creation of malignant cells. Skin tumors are classified into two types: malignant and benign. Squamous cell cancer (SCC), basal cell cancer (BCC), malignant melanoma, and dermatofibrosarcoma are all types of malignant skin cancers [10]. Malignant cutaneous adnexa, fibrous histiocytomas, Kaposi's sarcoma, and pleomorphic sarcoma are some of the less prevalent kinds. Malignant melanoma is especially harmful because it can spread to other regions of the body, a process known as metastasis, making it less prevalent but more lethal than other forms of skin cancer [11]. To address the constraints and limits of clinical evaluation, numerous computer-assisted diagnostic approaches [12], [13], [14], [15], [16], [17] have been developed to help dermatologists in identifying skin cancer, improving the diagnosis system's accuracy, efficiency, and impartiality.

In this paper, an optimized CNN model is used on the HAM10000 dataset to identify seven skin lesions implementing Grad-CAM, Grad-CAM++, SHAP, and LIME as explanation techniques with increased explanation and accuracy. We trained the model extensively to address the issue of imbalanced datasets and demonstrated their impact on model accuracy. In summary, we provide a robust model with improved accuracy when XAI approaches are used to diagnose skin cancer, and we make the following major contributions:

- Increased Model Transparency: The predictions of a deep learning model for skin lesions may be described using Grad-CAM and Grad-CAM++, which is an XAI technique. This improves not just the model's openness but also its accuracy, resulting in more trust in the diagnostic system and overall safety.
- Data Augmentation: We have trained 44, 666 dermoscopic pictures created from augmentation.
- Optimization and activation function: The model is trained by two optimization functions (Adam and RMSprop) and three activation functions (Relu, Swish, and Tanh)

The following is showing how the document is structured: Section II provides a review of the history and related studies, emphasizing the advantages and disadvantages of present approaches. Section III explains the created model, followed by Section IV's experimental analysis. Section V discusses the challenges to the study's validity. Section VI finishes this analysis by outlining future directions.

A. ARTIFICIAL INTELLIGENCE IN SKIN CANCER CLASSIFICATION

AI is being applied in a variety of medical applications, including skin cancer categorization. AI algorithms can diagnose skin lesions as benign or malignant by analyzing medical pictures such as dermatoscopic images. Dermatologists may find this useful because skin cancer can be difficult to detect, especially in its early stages.

Several studies have demonstrated that the performance of AI in skin cancer categorization is equivalent to that of professional dermatologists. It is crucial to highlight, however, that AI is not a replacement for a dermatologist's experience and clinical judgment, but rather a tool that can help with diagnosis.

Furthermore, it is critical to guarantee that AI algorithms employed in medical applications are verified, dependable, and interpretable to ensure that they make correct predictions and do not contribute to medical mistakes.

B. EXPLAINABLE ARTIFICIAL INTELLIGENCE IN SKIN CANCER CLASSIFICATION

In skin cancer classification, explainable artificial intelligence (XAI) refers to the employment of AI models that can give reasons for their diagnosis. This is critical in the field of medical diagnosis since skin cancer may be difficult to identify, and a clear grasp of the logic behind a diagnosis can be critical for patient treatment. Interpretable machine-learning models are one method that XAI is employed in skin cancer categorization.

To give insights into how the model makes its predictions, these models employ techniques such as feature significance analysis and decision tree visualization. Another method is to employ techniques like saliency maps and guided backpropagation to emphasize certain portions of an image that the model is utilizing to reach its diagnostic.

Furthermore, some XAI frameworks include an interface for domain experts to engage with the model, offering comments and explanations to help the model progress further.

Overall, the use of XAI in skin cancer classification can help improve the accuracy and trustworthiness of AI-assisted diagnoses, while also providing valuable information to healthcare professionals for making informed treatment decisions.

II. RELATED WORK

Zia et al. [18] improved the diagnosis of skin cancer by integrating extra convolution layers into two pre-trained deep learning models, MobileNetV2 as well as DenseNet201. The

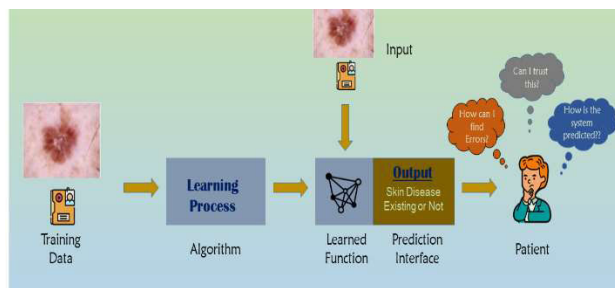


FIGURE 1. ML workflow with XAI: The model accurately explains the prediction and gives the answer “Why I should believe this output”, “How it predicts” and “How can I find an error”.

improved DenseNet201 model obtained 95.50% accuracy in identifying benign and malignant skin lesions, whereas the modified MobileNetV2 model reached 91.86% accuracy. The models were trained using an updated Kaggle dataset from the ISIC repository, which includes both benign and malignant categories. The augmentation procedure comprised introducing Gaussian noise to the dataset with a variance of 0.1. The study’s goal was to categorize skin lesions as benign or malignant, with the modified DenseNet201 model outperforming the modified MobileNetV2 model.

Gouda et al. [19] used DCNN models to detect two categories of primary tumors: malignant and benign. The model had an accuracy rate of 83.2%, compared to 83.7% for Resnet50, 85.8% for InceptionV3, and 84% for Inception Resnet. These findings are the sum of numerous repetitions. The ISIC 2018 dataset was utilized for model training and testing. ESRGAN was used to improve the pictures, which were then enhanced, normalized, and scaled during the pre-processing stage. The scientists successfully used a convolutional neural network to accurately categorize skin lesion photos as malignant or benign. They assessed the model’s performance using parameters such as accuracy, AUC, sensitivity, and specificity.

Dorj et al. [20] proposed a pre-trained AlexNet CNN model for extracting the features of the process as well an ECOC SVM classifier was used for forecasting skin cancer. The model achieved maximum accuracy of 95.1%, a sensitivity was 98.9% and specificity was 94.17% whereas minimum accuracy of 91.8%, a sensitivity of 96.9%, and a specificity of 96.9%. The results obtained during the study were impressive. The images were gathered from the internet (Google, Naver, Baidu, Bing). The images were cropped to reduce the noise for better results. The major objective of this study was to address the need for an intelligent and rapid classification system of skin cancer that uses highly-efficient deep convolutional neural networks.

Fu’adah et al. [21] used a CNN-based model to automatically detect skin cancer and benign tumor lesions. The suggested model used different optimizers, including SGD, RMSprop, Adam, and Adam, with Adam providing the highest performance, recognizing skin lesions with an accuracy of 83% and precision, recall, and F1-score of almost 1. The

findings of this investigation outperformed the previous skin cancer categorization method. Using enhanced data from the ISIC dataset, the model was trained to classify four types of skin cancer. The study’s purpose was to create a system for recognizing skin cancer and benign tumor lesions, improve classification accuracy and efficiency using a CNN-based technique, and evaluate the feasibility of deploying a CNN-based system as a screening system.

Barata et al. [22] used two alternative ways to construct a deep learning architecture for hierarchical diagnosis. ISIC 2017 provided the dataset for training, testing, and assessment. The architecture was created to identify three types of lesions: M, K, and N. 24 different network architectures were trained and assessed during the experiment. The hierarchical formulation was rated 90% with a BACC of 65.5%.

Natasha Nigar et al [23] used XAI and the ResNet-18 algorithm to construct a skin lesion categorization model. The model was verified by applying the International Skin Imaging Collaboration (ISIC) 2019 dataset, and it performed admirably, accurately detecting eight categories of skin lesions with a classification accuracy of 94.47%, precision of 93.57%, recall of 94.01%, an F1 score of 94.45%. The model was further investigated using the local interpretable model-agnostic explanations (LIME) framework to provide visual explanations that correspond with previous assumptions and general explanation best practices to further assess these predictions.

Ameri et al. [24] presented a deep-learning approach for skin cancer diagnosis using skin lesion photos. The model was made using the HAM1000 dermoscopy image library, which contained 3400 pictures including melanoma and non-melanoma lesions. The photos were divided into 860 cases of melanoma, 115 cases of dermatofibroma, 513 cases of basal cell carcinoma (BCC), 790 cases of benign keratoses, 795 cases of melanocytic nevi, and 327 cases of actinic keratoses and intraepithelial carcinoma (AKIEC). As AlexNet is the pre-trained model, the model used transfer learning and produced a ROC curve area of 0.91.

Senthil Kumar et al [25] proposed a Convolutional Neural Network (CNN)-based model for detecting and diagnosing skin cancer. The model was trained using the ISIC dataset, which has 2637 pictures. The dataset is preprocessed to an exhibit structure by using Image reshaping, resizing, and transformation. The training dataset is used to teach the model (CNN) how to recognize the test image. The model is 88% accurate and can differentiate between malignant and benign skin carcinoma cells.

To diagnose skin cancer, Stieler et al [26] suggested a Deep Neural Network (DNN)-based skin image classifier. In this paper, they show how to make explanations of an AI system for analyzing skin images more domain specific. The ABCD rule, a dermatologist’s diagnostic technique, is combined with the synthesis of Local Interpretable Model-agnostic Explanations (LIME). HAM10000 data set was used to train the model which contains microscopic pictures from many

sources of common pigmented skin lesions. There is no mention of accuracy.

Based on a fine-grained classification concept, Wei et al [27] created a lightweight skin cancer identification model with feature discrimination. A lesion classification network and a feature discrimination network share similar feature extraction modules in the proposed model. They created a lightweight semantic segmentation model of Dermo's copy image's lesion area, which can accomplish high-precision lesion area segmentation end-to-end without requiring costly image preparation processes. The ISBI 2016 data collection was used to train the model. There is no mention of precision here.

A study put forward by Nawaz et al [28] proposes an improved deep learning-based approach, namely the DenseNet77-based UNET model. The DenseNet77 network is introduced at the encoder unit of the UNET approach to computing a more representative set of image features. The calculated key points are later segmented by the decoder of the UNET model. The proposed approach is evaluated using two standard datasets, ISIC-2017 and ISIC-2018, achieving segmentation accuracies of 99.21% and 99.51%, respectively. The quantitative and qualitative results confirm that the proposed improved UNET approach is robust to skin lesion segmentation and can accurately recognize moles of varying colors and sizes.

Maqsood et al. [29] worked on a unified CAD model based on a deep learning framework. This approach involves preprocessing thermoscopic images using contrast enhancement and multiple exposure fusion. A custom 26-layer CNN is used for skin lesion segmentation, followed by transfer learning on pre-trained Xception, ResNet-50, ResNet-101, and VGG16 models. Deep features are fused using convolutional sparse image decomposition, and feature selection is done using univariate measurement and Poisson distribution. The selected features are classified using a multi-class support vector machine (MC-SVM). The proposed approach was applied to the HAM10000, ISIC2018, ISIC2019, and PH2 datasets, achieving higher accuracies (98.57%, 98.62%, 93.47%, and 98.98% respectively) than previous works.

A study done by Abayomi-Alli et al [30], proposes a novel data augmentation technique based on the covariant Synthetic Minority Oversampling Technique (SMOTE) to address the data scarcity and class imbalance problem in skin cancer detection. The proposed method is applied to dermoscopic images from the PH2 dataset, and the augmented images are used to train the SqueezeNet deep learning model. The results show a significant improvement in detecting melanoma with an accuracy of 92.18%, a sensitivity of 80.77%, a specificity of 95.1%, and an F1-score of 80.84% in binary classification. In multiclass classification, the proposed framework achieves an accuracy of 89.2% for atypical nevus detection and 66% for common nevus detection, outperforming some state-of-the-art methods in skin melanoma detection.

TABLE 1. Summary of some related papers' works in terms of accuracy, algorithm, dataset, and publication year.

Ref	Year	DL Algorithm	Dataset	Performance
[18]	2022	DenseNet201	Kaggle: ISIC archive	Accuracy: 95.50%
[19]	2022	Deep CNN	ISIC 2018	Accuracy: 83.2%
[20]	2018	AlexNet CNN	Internet (Google, Naver, Baidu, Bing)	Accuracy: 91.8% - 95.1%
[21]	2020	CNN	ISIC	Accuracy: 83%
[22]	2019	Multiple Hierarchical Architecture	ISIC 2017	BACC = 65.5%
[23]	2022	ResNet-18	ISIC 2019	Accuracy:94.4%, Precision:93.57%, Recall:94%, F1 Score:94.45%
[24]	2020	AlexNet	Map10000	Accuracy:84%, Sensitivity:81%, Specificity:88%
[25]	2022	CNN	ISIC	Accuracy:88%
[26]	2021	Deep Neural Network (DNN)	HAM1000	Not Mentioned
[27]	2020	lightweight CNN	ISBI 2016	Not Mentioned
[28]	2022	DenseNet77-based UNET	ISIC-2017 and ISIC-2018	Accuracy:99.21%, 99.51%
[29]	2023	CAD model based on a deep learning framework	HAM10000, ISIC2018, ISIC2019, and PH2 datasets	Accuracy:98.57%, 98.62%, 93.47%, and 98.98%
[30]	2021	SqueezeNet deep learning model	PH2 dataset.	Accuracy: 92.18%, sensitivity: 80.77%, specificity: 95.1%, and F1-score: 80.84 %

III. METHODOLOGIES

Deep learning has become a popular method in medical diagnostics, including skin cancer classification, due to its ability to effectively analyze large amounts of medical data, such as images of skin lesions. These algorithms can assist physicians in providing better care by accurately identifying and categorizing skin cancer patients.

The primary goals of using deep learning models for skin cancer classification are to improve the accuracy of diagnosis and the performance of categorization. To achieve these goals, an automated skin cancer classification system is typically created using a variety of deep learning models. These models are then evaluated using metrics such as accuracy, precision, recall, and F1 score to determine the best model for the task.

The enhanced approach for automatic categorization of skin cancer in this study involves classifying dermatoscopic

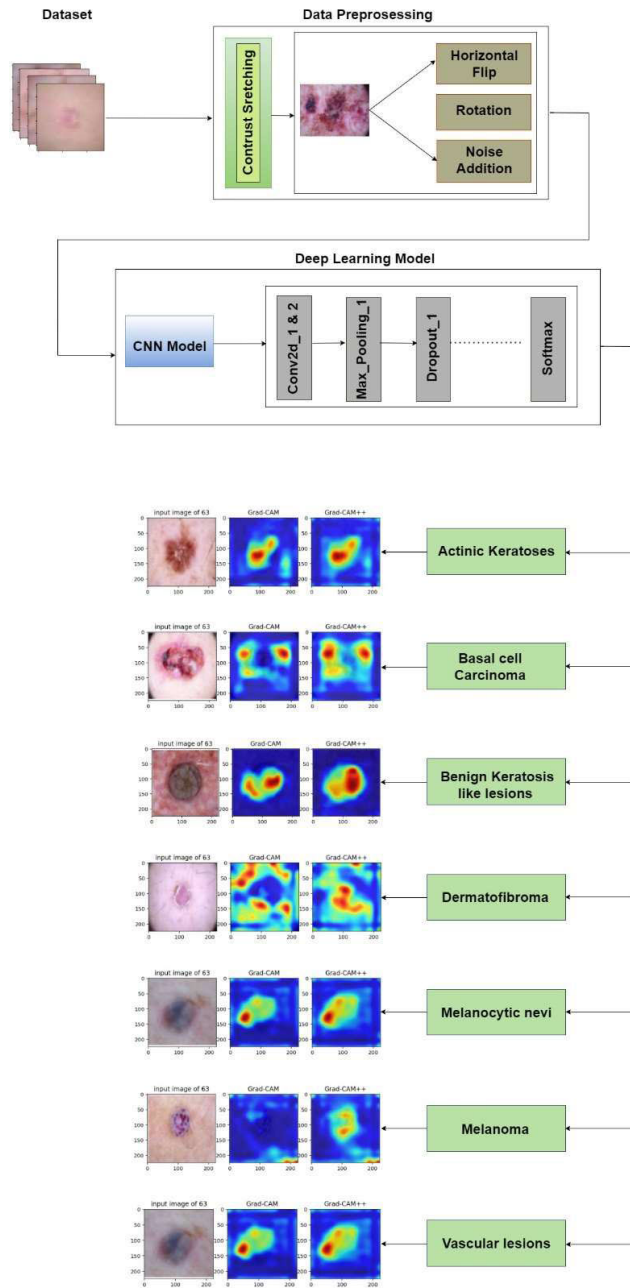


FIGURE 2. The proposed deep learning for skin cancer classifications. The augmentation technique is used for increasing the sample images, Then, cnn is used for extracting the features and training the model. The model classifies seven types of skin lesions.

images into four different categories. The model is developed through a five-step process: (1) obtaining a collection of dermatoscopic images for the skin cancer dataset; (2) pre-processing the dataset, which includes adjustments such as rescaling, resizing, and normalizing the data; (3) extracting features using layer-wise relevance propagation; (4) constructing a classifier using optimization algorithms on the extracted feature vectors; and (5) providing insight into the model's decision-making process through the use of Grad-CAM and Grad-CAM++ methods.

A. DATASET DESCRIPTION

The dataset is a crucial aspect of utilizing deep learning models in various applications. However, datasets are not always readily available, and high-quality, well-prepared datasets are even more scarce. Deep learning algorithms learn from the patterns and features present in the dataset and make predictions based on these learned patterns and features. Therefore, having a clean and well-prepared dataset is essential for achieving optimal performance with deep learning models. The dataset used in this work was obtained from Kaggle, a well-known scientific community website. The dataset is called HAM10000 and contains 10015 images, it is divided into seven groups.

B. DATA PREPROCESSING

Contrast stretching, also known as normalization, is a technique used to enhance the visual quality of an image by adjusting the image's contrast. It is often used to improve the visibility of features in an image, such as lesion spots in medical imaging. The technique adjusts the intensity values of the pixels in the image so that the minimum and maximum intensity values are mapped to the lowest and highest values in the output image, respectively. This can be done using a linear function or a non-linear function. In either case, the result is an image with increased contrast and improved visibility of features. A few contrast enhanced images are shown in Figure 5.

C. DATA AUGMENTATION

Data augmentation is a technique used to increase the number of training examples in a dataset. This is particularly important for deep learning models, which require a large amount of data to train effectively. There are various data augmentation techniques available in the literature, and different techniques may be suitable for different scenarios.

In this work, three different augmentation techniques are used: rotation, flipping, and noise addition. Rotation and flipping are scale-invariant operations, meaning they do not change the scale of the image. The images are rotated 15 and 45 degrees clockwise and anticlockwise, respectively, before being horizontally flipped. This increases the number of samples present in the dataset, while also introducing variations in the orientation of the images.

Before augmentation, the dataset size was 10015 but after augmentation, the number of images is 40,157 shown in Figure 6. After augmentation, the dataset is divided into three sections called the training set, validation set, and testing set. The split percentage is 70:15:15. So, every dataset has the same number of training, testing, and validation. The prediction will be learning well because of the same number of training images. The model has two optimization functions called “Adam” and “RmsProp”. In addition, the model also trained on three activation functions called “Relu”, “Swish” and “Tanh”.

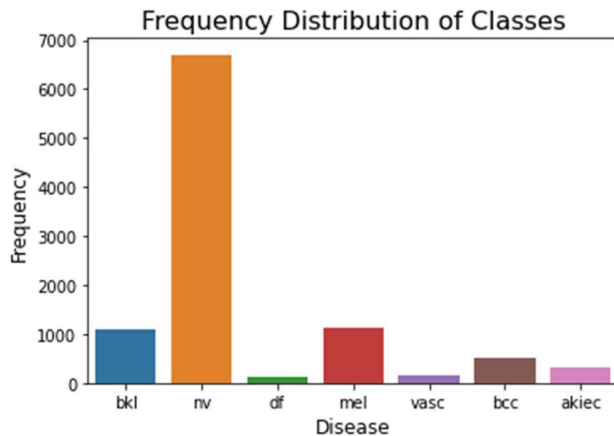


FIGURE 3. Number of samples per class.

TABLE 2. Dataset description.

S.No.	Name	Dtypes	Missing	Uniques
0	Lesion_id	Object	0	7470
1	Image_id	Object	0	10015
2	Dx	Object	0	7
3	Dx_type	Object	0	4
4	Age	Float64	57	18
5	Sex	Object	0	3
6	Localization	Object	0	15
7	Path	Object	0	10015
8	Cell_type	Object	0	7
9	Cell_type_id_x	Int8	0	7

D. EXPLORING FEATURES/TARGET

Figures 8 to 12 represent the visualization of the features in the dataset. Dataset visualization is important in deep learning because it helps to understand the structure and distribution of the data that the model is being trained on. This information can be used to guide preprocessing steps such as normalization, to identify potential issues such as class imbalances, and to gain a better understanding of the relationships between the features in the data. Dataset visualization can also help to identify potential problems in the data such as outliers or missing values, which can affect the performance of the model. Additionally, dataset visualization can provide a visual representation of the problem the model is trying to solve, which can be useful in communicating results and building a shared understanding between team



FIGURE 4. Sample Images from the data set.

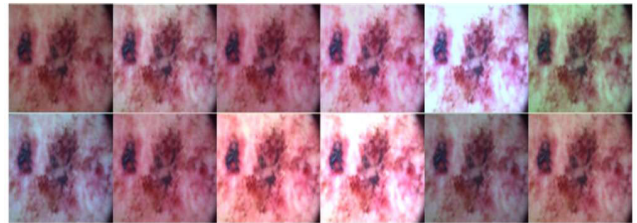


FIGURE 5. Some contrast images from the original sample.

members. Overall, dataset visualization plays an important role in the development and training of deep learning models by helping to identify and address issues in the data.

E. CORRELATION HEATMAPS

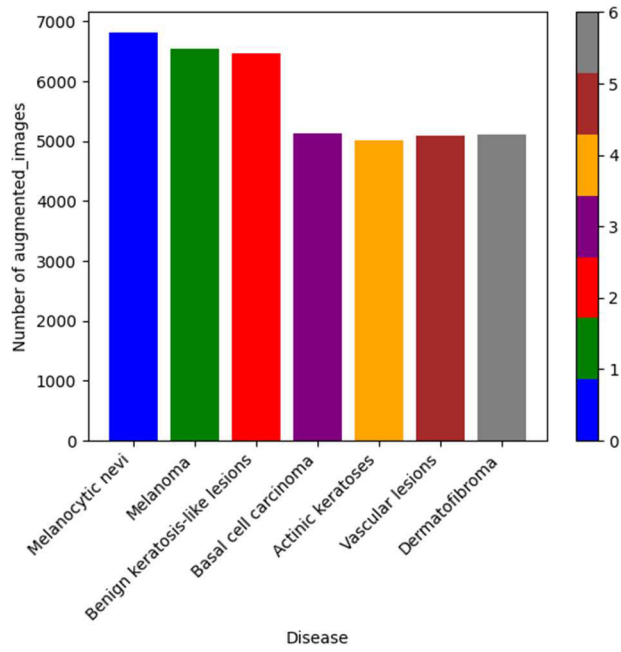
A correlation heatmap is a useful tool to graphically represent how two features are related to each other. Depending upon the data types of the features, we need to use the appropriate correlation coefficient calculation methods. Examples are Pearson's correlation coefficient, point biserial correlation, cramers' correlation, etc.

F. TRAIN TEST SPLIT

After balancing the dataset, the partitioning process began. The train-test split approach was utilized, and the dataset was separated into three parts: the training set, the validation set, and the test set. The training set was used to train the machine learning model, the validation set to validate it, and the test set to evaluate its performance. In our case, we divided our

TABLE 3. Details description of samples.

Disease	Original Images	Augmented Images	Training images	Validation Images	Testing Images
Melanocytic nevi	6705	6812	4584	1124	1104
Melanoma	1113	6543	4580	981	981
Benign keratosis-like lesions	1099	6456	4519	968	968
Basal cell carcinoma	514	5123	3586	768	768
Actinic keratoses	327	5012	3508	717	717
Vascular lesions	142	5099	3569	765	765
Dermatofibroma	115	5112	3578	767	767

**FIGURE 6.** Augmented image distribution per class.

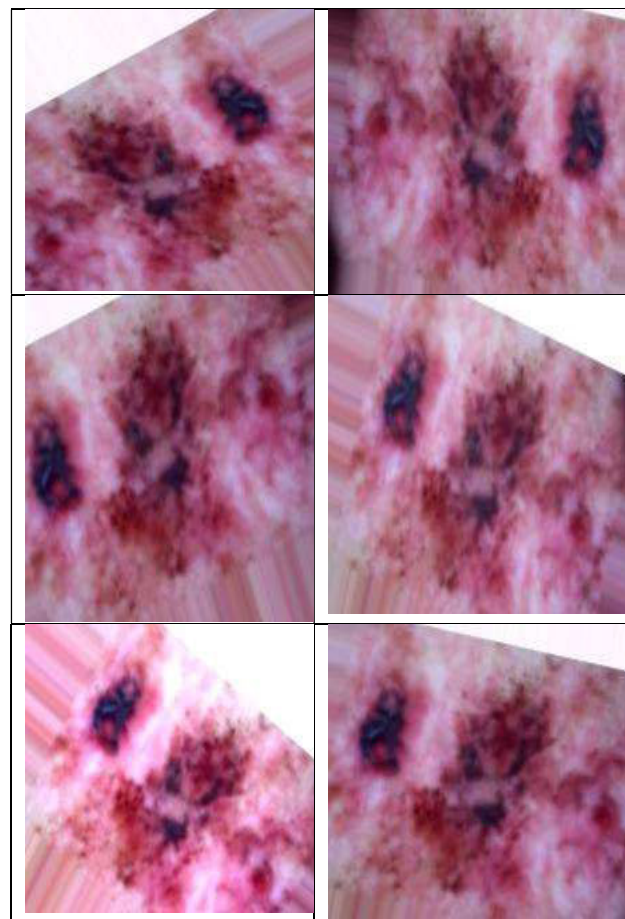
set into 70:15:15. The number of training samples is 31,264 (70%), and the testing samples are 5696 (15%)

Training	Testing	Validation
31,264	5696	5696

G. IMPLEMENTATION OF CNN

Table 5 represents the architecture value of the proposed CNN model. The image size is $100 \times 100 \times 3$ where the first 100 is image height, the second 100 is weight, and 3 is the channel.

Block 1: The images pass through the two convolutional layers with a kernel size of 3×3 , strides 1, ReLu activation function. The output shape is $(100,100,32)$. After using the

TABLE 4. Samples after data augmentation techniques.

Maxpooling_1 layer of strides 1 and dropout layers, the block 1 shape is $(50,50,32)$ where 32 is the filter size.

Block 2: The output of block 1 is passing block 2 where two convolutional layers with a kernel size of 3 and one max pooling layer of strides of 2 and one dropout layer. Before max pooling, the size is $(50,50,64)$, and after max pooling operation, the size is $(25,25,64)$ where the filter size is 64.

Other layers: We flatten the output of block 2 from $(25,25,64)$ to 40000. Then we use one dense layer of size 128 and a dropout layer. Finally, we use a 7-dense layer with a SoftMax activation function. As an optimization function, we use Adam where we got the highest accuracy of almost 82%.

H. X-AI: EXPLAINABLE ARTIFICIAL INTELLIGENCE IN MODEL EXPLANATION

XAI (Explainable Artificial Intelligence) is a field of study that seeks to develop AI systems that can provide clear and intelligible explanations for their predictions and judgments. The goal of XAI is to create AI systems that are open and responsible, guaranteeing that people can trust and grasp their judgments. A critical feature of XAI is a model explanation, which refers to an AI system's capacity to explain

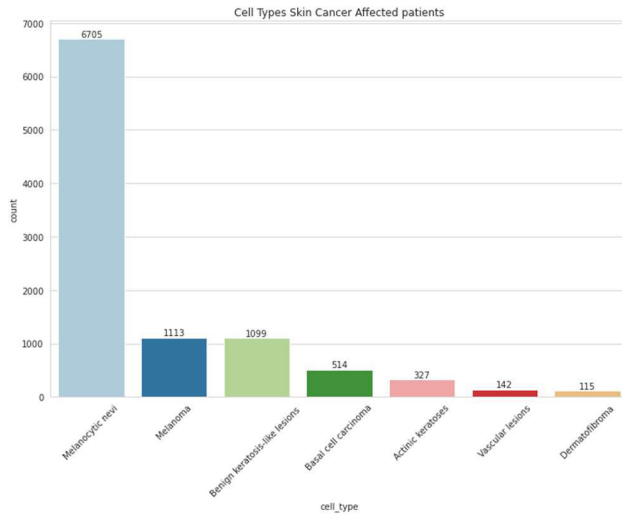


FIGURE 7. Cell types skin cancer affected patients.

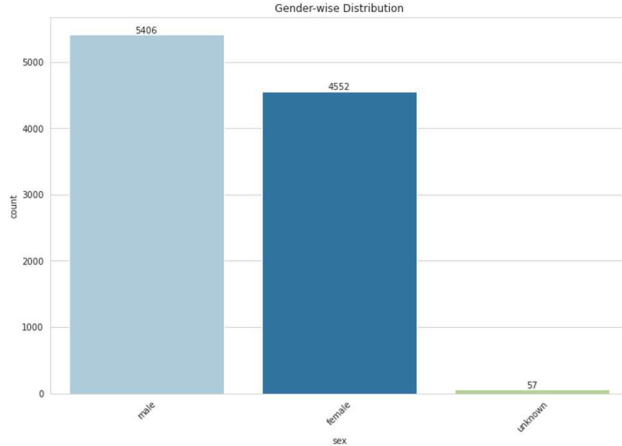


FIGURE 8. Gender-wise distribution.

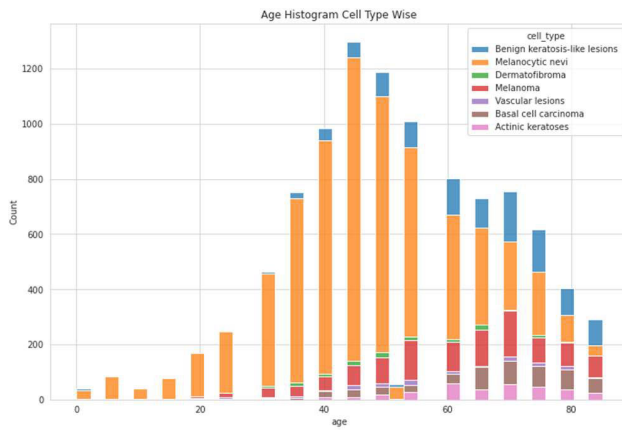


FIGURE 9. Cell type wise age histogram.

its predictions or conclusions. Some common methods for explaining machine learning models include Grad-CAM and Grad-CAM++ [31], [32].

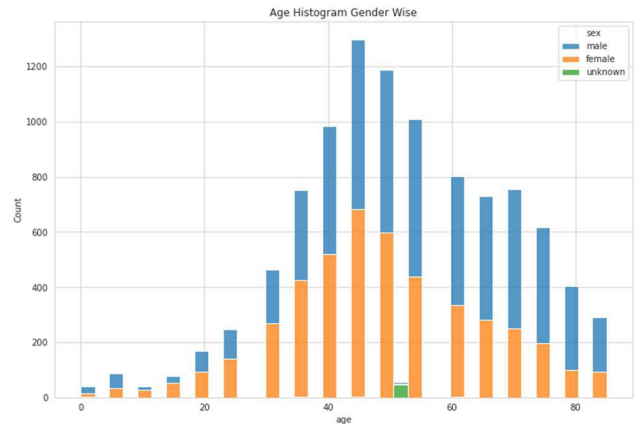


FIGURE 10. Age histogram gender wise.

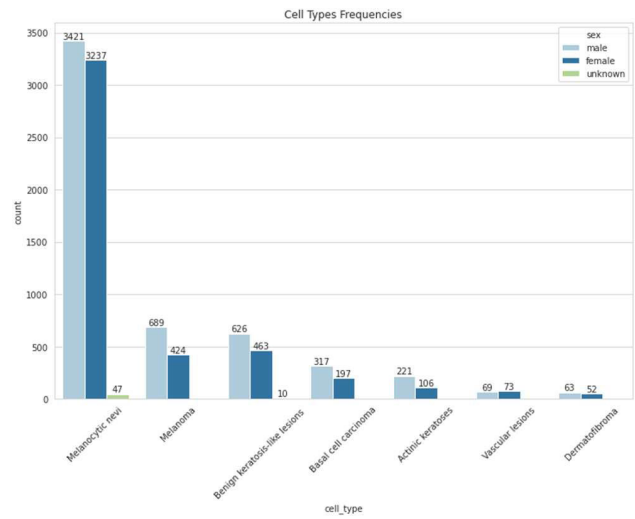


FIGURE 11. Cell type frequency gender wise.

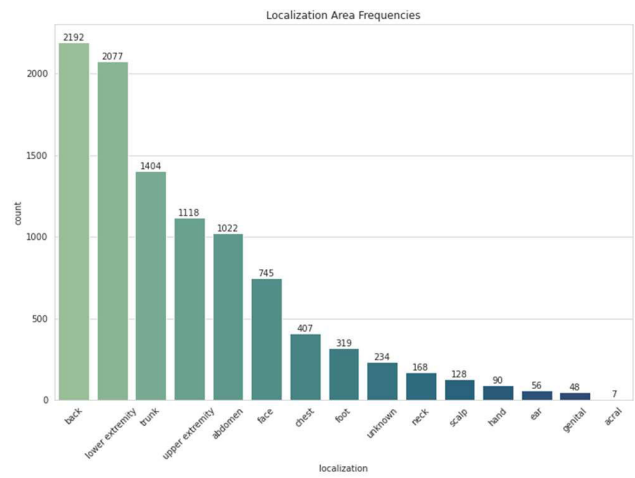


FIGURE 12. Location area frequencies.

We can implement Grad-CAM in three steps as follows:

Step 1: Compute Gradient: Compute the gradient y_c concerning the feature map activations A^k of a convolution layer

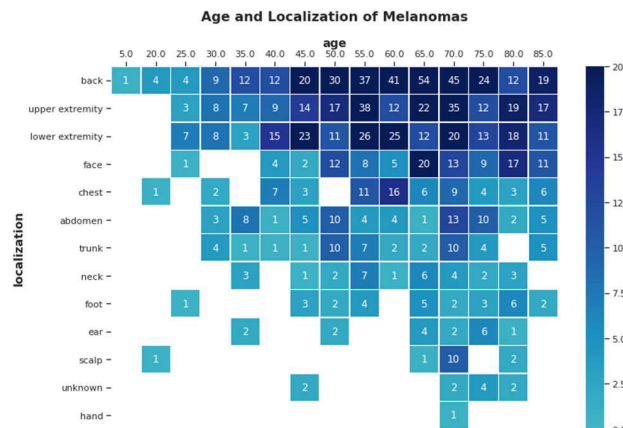


FIGURE 13. Age and localization of melanomas.

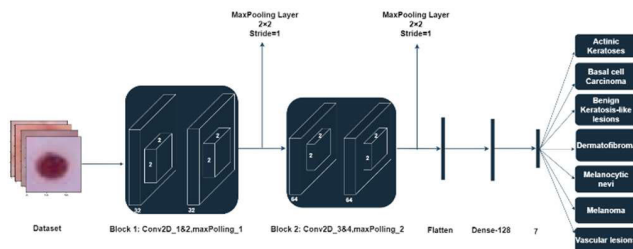


FIGURE 14. Proposed CNN model architecture.

TABLE 5. Model structure: layer, shape, and parameters.

	Layer (type)	Output shape	Param#
Block - 1	Conv2D_1	(100,100,32)	896
	Conv2D_2	(100,100,32)	9248
	MaxPooling_1	(50,50,32)	0
	Dropout_1	(50,50,32)	0
Block - 2	Conv2D_3	(50,50,64)	18496
	Conv2D_4	(50,50,64)	36928
	MaxPooling_2	(25,25,64)	0
	Dropout_2	(25,25,64)	0
Others	Flatten	(40000)	0
	Dense_1	(128)	5120128
	Dropout_3	(128)	0
Total params: 5,186,599			
Trainable params: 5,186,599			
Non-trainable params: 0			

i.e. $\frac{\delta y^c}{\delta A^k}$. Suppose, we have three feature maps denoted by A^1, A^2, A^3 and want to get the gradient value of class “Vascular” so here $y_c = y_{vas}$.

Now Calculate the gradient of the score for Vascular lesions concerning the feature maps of the last convolutional layer.

$$\frac{\delta y^{vas}}{\delta A^k} = \frac{\delta y^{vas}}{\delta A^1} + \frac{\delta y^{vas}}{\delta A^2} + \frac{\delta y^{vas}}{\delta A^3} \quad (1)$$

Step 2: Calculate Alphas by Averaging Gradients: Global average pool the gradients over the width dimension (index by i) and the height dimension (index by j) to obtain neuron

importance weight i.e α_k^{vas}

$$\alpha_k^{vas} = \frac{1}{Z} \sum_i \sum_j \frac{\delta y^{vas}}{\delta A_{ij}^k} \quad (2)$$

Calculating α by averaging.

$$\begin{aligned} \frac{\delta y^{vas}}{\delta A^1} &= \text{averaging}(\alpha_{k=1}^{vas}) \\ \frac{\delta y^{vas}}{\delta A^2} &= \text{averaging}(\alpha_{k=2}^{vas}) \\ \frac{\delta y^{vas}}{\delta A^3} &= \text{averaging}(\alpha_{k=3}^{vas}) \end{aligned}$$

Step 3: Calculate Final Grad-CAM Heatmap: Perform a weighted combination of the feature map activations A^k where here the weights are α_k^{vas} just calculated.

$$L_{Grad-CAM}^{vas} = \text{ReLU}(\sum_k \alpha_k^{vas} A^k) \quad (3)$$

where Here,

$$Grad - CAM^{vas} = \alpha_1 A^1 + \alpha_2 A^2 + \alpha_3 A^3 i.e \sum_k \alpha_k^{vas} A^k \quad (4)$$

Grad-CAM is an algorithm that can be used to generate visual explanations for the predictions of a deep learning model, by highlighting the regions of the input image that are most important for the model’s prediction. However, one limitation of Grad-CAM is that it can only generate a coarse heatmap because it only uses the gradients of the target class concerning the convolutional layers of the model to generate the heatmap. Grad-CAM++ addresses this limitation by using guided backpropagation to generate guided feature maps, which retain more spatial information than the feature maps used in Grad-CAM. The dot product of the guided feature maps and the gradients of the target class is then taken to generate the heatmap, similar to Grad-CAM. By using guided backpropagation, Grad-CAM++ can generate a more detailed heatmap that highlights the specific regions of the input image that are most important for the model’s prediction. This can be useful for understanding the reasons behind the model’s predictions, and for debugging and improving the model.

$$y^{vas} = \sum_k \{ \sum_a \sum_b \alpha_{ab}^{K,vas} \cdot \text{relu}(\frac{\delta y^{vas}}{\delta A_{ab}^k}) \} [\sum_i \sum_j A_{ij}^k] \quad (5)$$

These equations from 1 to 5 are only for one particular class using Grad-CAM and Grad-CAM++. If we want to explain other models as well, we can use the same equations to visualize the important features. The visualization of all classes through both of the techniques showing in Table 5.

TABLE 6. Most common machine learning evaluation metrics.

		Predicted values		
		True	False	
Actual	True	True Positive (TP)	False Negative (FN) Type 1 Error	$\text{Recall} = \text{Sensitivity} = \frac{TP}{TP+FN}$
	False	False Positive (FP) Type 1 Error	True Negative (TN)	$\text{Specificity} = \frac{TN}{TN+FP}$
		$\text{Accuracy} = \frac{TP+TN}{TP+TN+FP+FN}$ $F1 = \frac{2 \times \text{Precision} \times \text{Recall}}{\text{Precision} + \text{Recall}}$		
		$\text{Precision} = \frac{TP}{TP+FP}$		

TABLE 7. Training, validation, and testing accuracy/loss of three activation functions and two optimization functions.

Activation Function	Relu	Optimization Function			
		Adam		RMSprop	
	Training acc/Loss	81.24	0.47	72.52	0.76
	Vali. acc/Loss	78.06	0.68	73.40	0.73
	Test acc/Loss	78.79	0.69	72.68	0.76
	Training acc/Loss	80.41	0.50	80.99	0.50
	Vali. acc/Loss	79.91	0.77	77.79	0.62
	Test acc/Loss	77.40	0.81	75.50	0.68
Swish	Training acc/Loss	67.18	1.14	79.12	0.55
	Vali. acc/Loss	66.62	1.12	70.38	0.79
	Test acc/Loss	65.86	1.14	71.98	0.78
Tanh	Training acc/Loss	65.86	1.14	71.98	0.78
	Vali. acc/Loss	65.86	1.14	71.98	0.78
	Test acc/Loss	65.86	1.14	71.98	0.78

IV. RESULTS

A. METRICS

In deep learning, a metric is a measure of the performance of a DL model. Metrics are used to evaluate the accuracy, effectiveness, and efficiency of a model, and to compare the performance of different models. Many different metrics can be used in deep learning, and the specific metric that is used will depend on the specific task and the requirements of the application. Some common metrics for deep learning include:

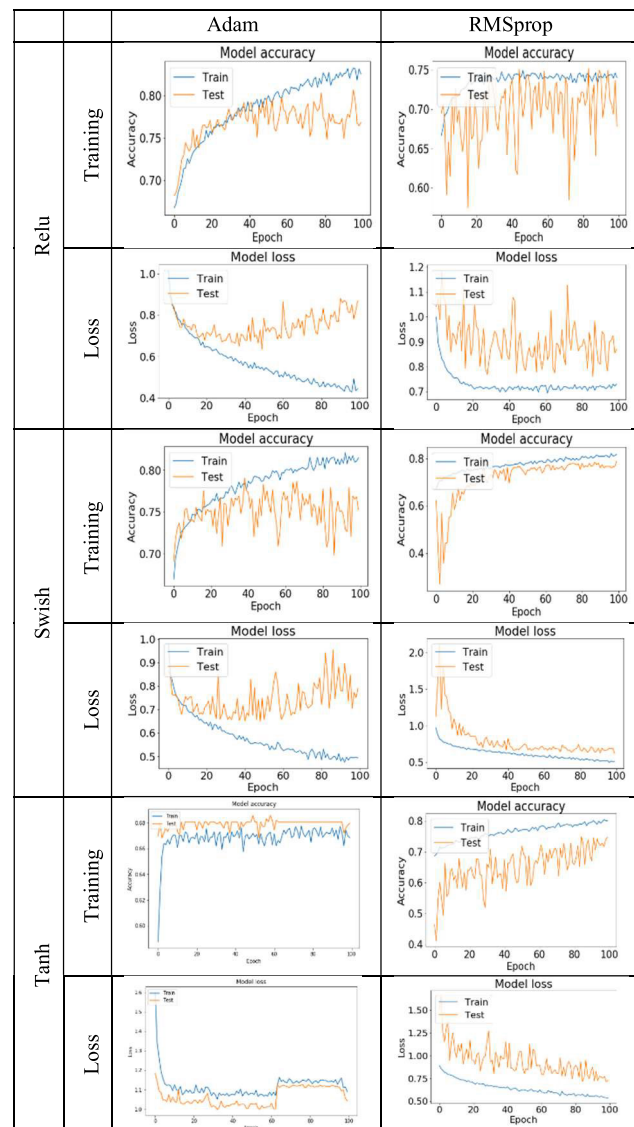
Classification accuracy: This is the percentage of correct predictions made by the model, and is often used as the primary metric for classification tasks.

Precision and recall: These metrics are used to evaluate the model's ability to identify positive examples (e.g. detecting cancer in a medical diagnosis task). Precision is the percentage of true positive predictions made by the model, while recall is the percentage of actual positive examples that were correctly identified [33].

F1 score: The F1 score is the harmonic mean of accuracy and recall, and it represents a balance between the two. It is frequently used as a single statistic to assess the effectiveness of a classification model [34].

B. CLASSIFICATION MODEL RESULTS

In Table 7 shown, training, validation, and testing accuracy/loss is shown for two optimization functions and three activation functions. Based on the performance table, the highest training accuracy is 81.24% get from

TABLE 8. Training, validation, and testing accuracy/loss curve of three activation functions and two optimization functions.**FIGURE 15.** Role of explainer to enhance the interpretability.

“ReLU+Adam” where ReLU is the activation function and Adam is the optimization function. This model not only

TABLE 9. Confusion matrix of three activation functions and two optimization functions.

		Confusion							
		Confusion matrix							
Relu	Adam	Original Class							
		0	10.000	3.000	7.000	0.000	4.000	0.000	0.000
		1	6.000	20.000	8.000	2.000	6.000	0.000	0.000
		2	2.000	4.000	51.000	0.000	27.000	0.000	0.000
		3	2.000	1.000	4.000	0.000	2.000	0.000	0.000
		4	1.000	1.000	24.000	1.000	500.000	4.000	0.000
		5	2.000	0.000	25.000	0.000	45.000	29.000	0.000
Relu	RMSprop	6	0.000	0.000	0.000	0.000	1.000	0.000	5.000
		0	1	2	3	4	5	6	0
		Predicted Class							
		Confusion matrix							
		0	3.000	8.000	11.000	0.000	2.000	0.000	0.000
		1	0.000	33.000	7.000	0.000	2.000	0.000	0.000
		2	1.000	9.000	44.000	0.000	26.000	4.000	0.000
Swish	Adam	3	0.000	4.000	3.000	0.000	2.000	0.000	0.000
		4	2.000	14.000	19.000	0.000	462.000	31.000	3.000
		5	2.000	4.000	21.000	0.000	45.000	28.000	1.000
		6	0.000	0.000	0.000	0.000	0.000	6.000	0.000
		0	1	2	3	4	5	6	0
		Predicted Class							
		Confusion matrix							
Swish	RMSprop	0	12.000	2.000	6.000	0.000	3.000	1.000	0.000
		1	9.000	21.000	4.000	1.000	5.000	2.000	0.000
		2	6.000	1.000	47.000	0.000	22.000	8.000	0.000
		3	2.000	2.000	0.000	1.000	4.000	0.000	0.000
		4	3.000	2.000	12.000	0.000	499.000	14.000	1.000
		5	3.000	2.000	17.000	0.000	53.000	25.000	1.000
		6	0.000	0.000	0.000	0.000	0.000	1.000	5.000
Tanh	Adam	0	11.000	5.000	4.000	0.000	3.000	1.000	0.000
		1	6.000	19.000	10.000	1.000	4.000	2.000	0.000
		2	1.000	3.000	54.000	0.000	22.000	4.000	0.000
		3	0.000	1.000	4.000	3.000	1.000	0.000	0.000
		4	2.000	1.000	15.000	2.000	482.000	28.000	1.000
		5	4.000	0.000	17.000	1.000	40.000	39.000	0.000
		6	0.000	0.000	0.000	0.000	0.000	1.000	5.000
Tanh	RMSprop	0	0.000	0.000	0.000	0.000	24.000	0.000	0.000
		1	0.000	0.000	0.000	0.000	42.000	0.000	0.000
		2	0.000	0.000	0.000	0.000	84.000	0.000	0.000
		3	0.000	0.000	0.000	0.000	9.000	0.000	0.000
		4	0.000	0.000	0.000	0.000	531.000	0.000	0.000
		5	0.000	0.000	0.000	0.000	101.000	0.000	0.000
		6	0.000	0.000	0.000	0.000	6.000	0.000	0.000

TABLE 10. Precision matrix of three activation functions and two optimization functions.

		Precision							
		Precision matrix							
Relu	Adam	Original Class							
		0	0.435	0.103	0.059	0.000	0.007	0.000	0.000
		1	0.261	0.690	0.067	0.667	0.010	0.000	0.000
		2	0.087	0.138	0.429	0.000	0.046	0.000	0.000
		3	0.087	0.034	0.034	0.000	0.003	0.000	0.000
		4	0.043	0.034	0.202	0.333	0.855	0.121	0.000
		5	0.087	0.000	0.210	0.000	0.077	0.879	0.000
Relu	RMSprop	6	0.000	0.000	0.000	0.000	0.002	0.000	1.000
		0	1	2	3	4	5	6	0
		Predicted Class							
		Precision matrix							
		0	0.375	0.111	0.105	0.004	0.000	0.000	0.75
		1	0.000	0.458	0.067	0.004	0.000	0.000	0.60
		2	0.125	0.125	0.419	0.048	0.063	0.000	0.45
Swish	Adam	3	0.000	0.056	0.029	0.004	0.000	0.000	0.30
		4	0.250	0.194	0.181	0.857	0.492	0.300	0.15
		5	0.250	0.056	0.200	0.083	0.444	0.100	0.00
		6	0.000	0.000	0.000	0.000	0.000	0.600	0.00
		0	1	2	3	4	5	6	0
		Predicted Class							
		Precision matrix							
Swish	RMSprop	0	0.343	0.067	0.070	0.000	0.005	0.020	0.000
		1	0.257	0.700	0.047	0.500	0.009	0.039	0.000
		2	0.171	0.033	0.547	0.000	0.038	0.157	0.000
		3	0.057	0.067	0.000	0.500	0.007	0.000	0.000
		4	0.086	0.067	0.140	0.000	0.852	0.275	0.143
		5	0.086	0.067	0.198	0.000	0.090	0.490	0.143
		6	0.000	0.000	0.000	0.000	0.000	0.020	0.714
Tanh	Adam	0	0.458	0.172	0.038	0.000	0.005	0.013	0.000
		1	0.250	0.655	0.096	0.143	0.007	0.027	0.000
		2	0.042	0.103	0.519	0.000	0.040	0.053	0.000
		3	0.000	0.034	0.038	0.429	0.002	0.000	0.000
		4	0.083	0.034	0.144	0.286	0.873	0.373	0.167
		5	0.167	0.000	0.163	0.143	0.072	0.520	0.000
		6	0.000	0.000	0.000	0.000	0.000	0.013	0.833
Tanh	RMSprop	0	0.030	0.053	0.105	0.011	0.066	0.127	0.015
		1	0.000	0.000	0.000	0.000	0.000	0.008	0.000
		2	0.348	0.143	0.046	0.000	0.007	0.040	0.000
		3	0.391	0.679	0.059	0.100	0.005	0.000	0.143
		4	0.130	0.036	0.401	0.100	0.031	0.040	0.000
		5	0.043	0.000	0.013	0.300	0.005	0.000	0.000
		6	0.087	0.036	0.276	0.400	0.861	0.280	0.000
		0	0.000	0.000	0.007	0.000	0.000	0.000	0.714
		1	0.000	0.000	0.000	0.000	0.000	0.000	0.000
		2	0.000	0.000	0.000	0.000	0.000	0.000	0.000
		3	0.000	0.000	0.000	0.000	0.000	0.000	0.000
		4	0.000	0.000	0.000	0.000	0.000	0.000	0.000
		5	0.000	0.000	0.000	0.000	0.000	0.000	0.000
		6	0.000	0.000	0.000	0.000	0.000	0.000	0.000

TABLE 11. Recall matrix of three activation functions and two optimization functions.

		Recall							
		Recall matrix							
Relu	Adam	Recall matrix							
		Original Class 0	0.417	0.125	0.292	0.000	0.167	0.000	0.000
		1	0.143	0.476	0.190	0.048	0.143	0.000	0.000
		2	0.024	0.048	0.607	0.000	0.321	0.000	0.000
		3	0.222	0.111	0.444	0.000	0.222	0.000	0.000
		4	0.002	0.002	0.045	0.002	0.942	0.008	0.000
		5	0.020	0.000	0.248	0.000	0.446	0.287	0.000
		6	0.000	0.000	0.000	0.000	0.167	0.000	0.833
		0	1	2	3	4	5	6	0.0
Swish	Adam	Recall matrix							
		Original Class 0	0.125	0.333	0.458	0.000	0.083	0.000	0.000
		1	0.000	0.786	0.167	0.000	0.048	0.000	0.000
		2	0.012	0.107	0.524	0.000	0.310	0.048	0.000
		3	0.000	0.444	0.333	0.000	0.222	0.000	0.000
		4	0.004	0.026	0.036	0.000	0.870	0.058	0.006
		5	0.020	0.040	0.208	0.000	0.446	0.277	0.010
		6	0.000	0.000	0.000	0.000	0.000	0.000	1.000
		0	1	2	3	4	5	6	0.0
Tanh	Adam	Recall matrix							
		Original Class 0	0.500	0.083	0.250	0.000	0.125	0.042	0.000
		1	0.214	0.500	0.095	0.024	0.119	0.048	0.000
		2	0.071	0.012	0.560	0.000	0.262	0.095	0.000
		3	0.222	0.222	0.000	0.111	0.444	0.000	0.000
		4	0.006	0.004	0.023	0.000	0.940	0.026	0.002
		5	0.030	0.020	0.168	0.000	0.525	0.248	0.010
		6	0.000	0.000	0.000	0.000	0.000	0.167	0.833
		0	1	2	3	4	5	6	0.0
Relu	RMSprop	Precision matrix							
		Original Class 0	0.458	0.172	0.038	0.000	0.005	0.013	0.000
		1	0.250	0.655	0.096	0.143	0.007	0.027	0.000
		2	0.042	0.103	0.519	0.000	0.040	0.053	0.000
		3	0.000	0.034	0.038	0.429	0.002	0.000	0.000
		4	0.083	0.034	0.144	0.286	0.873	0.373	0.167
		5	0.167	0.000	0.163	0.143	0.072	0.520	0.000
		6	0.000	0.000	0.000	0.000	0.000	0.013	0.833
		0	1	2	3	4	5	6	0.0
Swish	RMSprop	Recall matrix							
		Original Class 0	0.000	0.000	0.000	0.000	1.000	0.000	0.000
		1	0.000	0.000	0.000	0.000	1.000	0.000	0.000
		2	0.000	0.000	0.000	0.000	1.000	0.000	0.000
		3	0.000	0.000	0.000	0.000	1.000	0.000	0.000
		4	0.000	0.000	0.000	0.000	1.000	0.000	0.000
		5	0.000	0.000	0.000	0.000	1.000	0.000	0.000
		6	0.000	0.000	0.000	0.000	1.000	0.000	0.000
		0	1	2	3	4	5	6	0.0
Tanh	RMSprop	Recall matrix							
		Original Class 0	0.333	0.167	0.292	0.000	0.167	0.042	0.000
		1	0.214	0.452	0.214	0.024	0.071	0.000	0.024
		2	0.036	0.012	0.726	0.012	0.202	0.012	0.000
		3	0.111	0.000	0.222	0.333	0.333	0.000	0.000
		4	0.004	0.002	0.079	0.008	0.895	0.013	0.000
		5	0.000	0.030	0.297	0.010	0.495	0.158	0.010
		6	0.000	0.000	0.167	0.000	0.000	0.000	0.833
		0	1	2	3	4	5	6	0.0

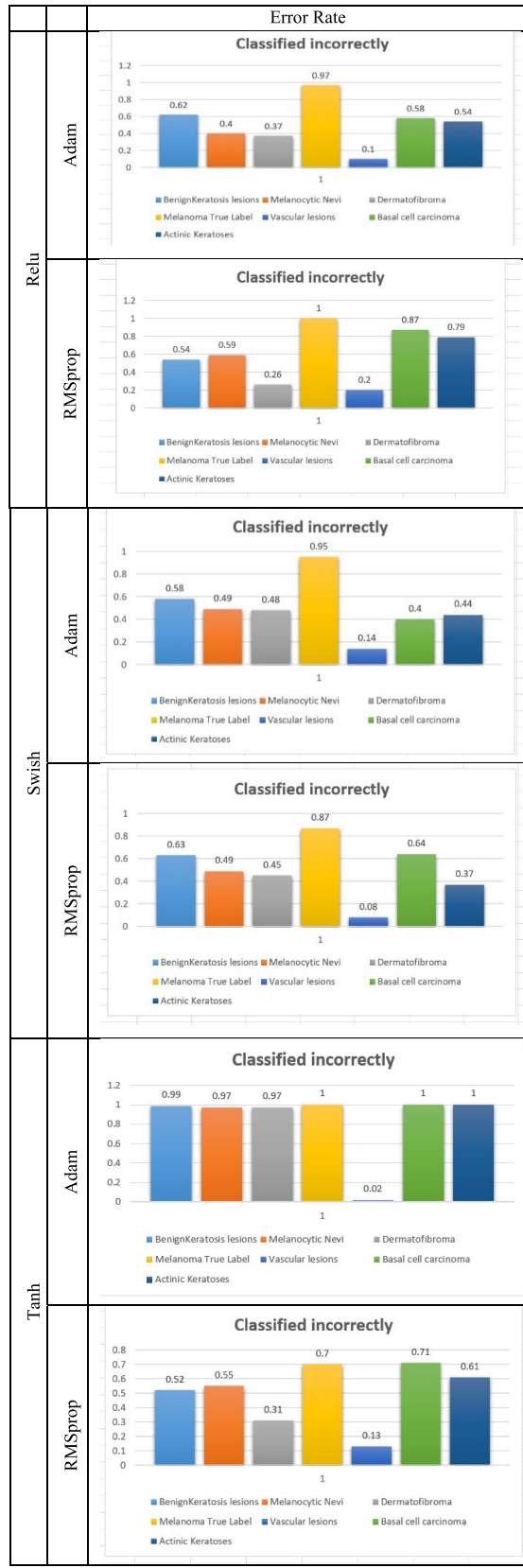
TABLE 12. Error rate of three activation functions and two optimization functions.

TABLE 13. Visualization of four class images through Grad-CAM and Grad-CAM++.

Class	Visualization		
Actinic Keratoses	input image	Grad-CAM	Grad-CAM++
Basal cell Carcinoma	input image	Grad-CAM	Grad-CAM++
Benign Keratosis-like lesions	input image	Grad-CAM	Grad-CAM++
Dermatofibroma	input image	Grad-CAM	Grad-CAM++
Melanocytic nevi	input image	Grad-CAM	Grad-CAM++
Melanoma	input image	Grad-CAM	Grad-CAM++
Vascular lesions	input image	Grad-CAM	Grad-CAM++

gives the highest accuracy but also provides less error almost 0.47. The second highest training accuracy gets from the “Swish+RMSprop” model. The training accuracy is near 81% and the error rate is 0.50.

Testing and validation performance are also important factors to choose an optimized model. In this research work, both works had been done. As the dataset is divided into three sets, the validation and testing are two of them. The testing accuracy is neat to 79% whereas the validation accuracy is 78.06% performed by “ReLU+Adam”. The difference in

loss error between validation and testing is almost 1 which means the model performance is stable.

The accuracy and loss curves are shown in Table 8. As we have given the performance in Table 7 where the best performance got from “ReLU+Adam” and the second-best performance is from “Swish+RMSprop”. According to the curve performance, it is clear that the “ReLU+Adam” performance is slightly higher than the second one. The best training curve has a healthy difference between training and testing accuracy whereas the “Swish+RMSprop” has less difference between training and testing curves.

Tables 9, 10, and 11 are the confusion, precision, and recall respectively. We have a total of seven classes that are mentioned as 0 to 6. The confusion matrix compares its actual values with predicted values. According to this confusion matrix, the accuracy of the model performance can be calculated. The equations are mentioned in Table 6. In addition, precision is used for calculating the true prediction values where the recall provides the performance of true negatives. Furthermore, we can also calculate the error rate which is classified incorrectly. In Table 12 the error rate with specific values for a specific class is mentioned which will give information on incorrect classification values.

Table 12 depicts the error rate for every model and every target class. The training and test curve is the giving the accuracy and the loss curve shows the error rate per epoch. We train our models with 100 epochs. We have more error rates in “Tanh+Adam” and “Tanh+RMSprop” whereas we have very less errors in “Swish+RMSprop”.

C. X-AI PERFORMANCE ON MACHINE LEARNING

Patients and physicians who are not from a technical background will not be able to understand any prediction of the model’s model, Explainable Artificial Intelligence; X-AI will be the one to explain specific forecasts to them. Frequently, the Grad-CAM approach is used to describe machine learning models but here we also consider Grad-CAM++ for better understanding.

These are the output of Explainable AI techniques called Grad-CAM and Grad-CAM++. The proposed CNN model provides better accuracy with a better explanation of specific classification. The explainability of this model is shown in Table 13 where all seven class images are present. Grad-CAM can explain the important feature by highlighting the disease areas but Grad-CAM++ performs better as it can explain more important features. From this visualization, the prediction output can be understood easily as to why and how the model classify.

Figure 16. is a filter visualization that shows the weights of the filters in a convolutional layer of the network. These visualizations help us to understand what patterns or feature the filters are detecting in the input data. Here, we only consider which layer size is 4 because those layers consist of convolutional, max pooling, and dropout layers. For instance, conv2d, max_pooling2d, conv2d_1 32, max_pooling2d_1,

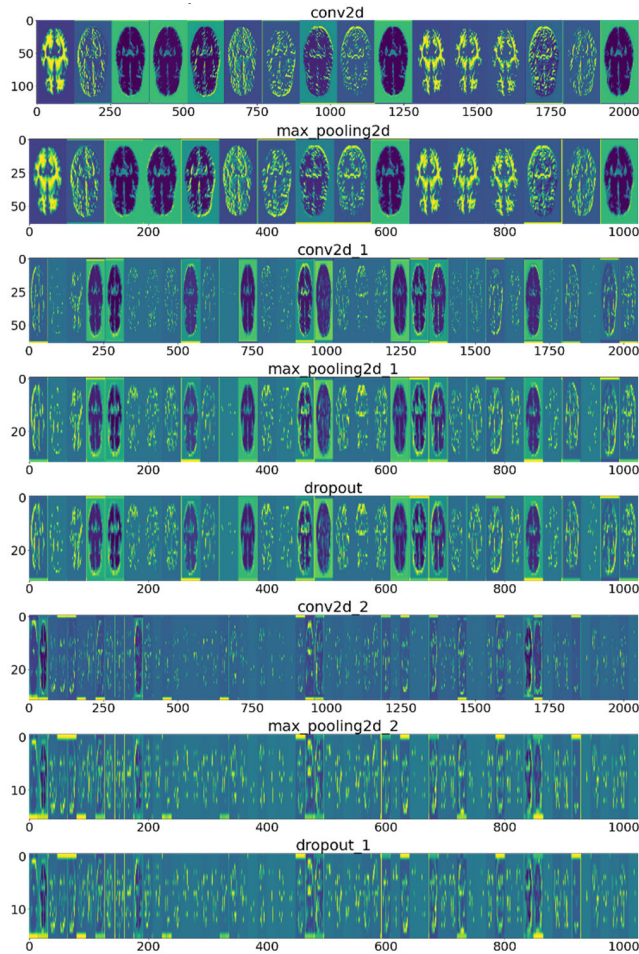


FIGURE 16. Layer-wise visualization.

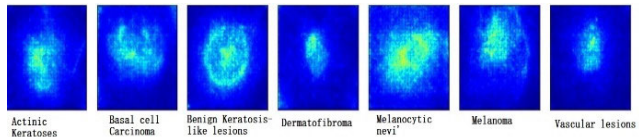


FIGURE 17. Saliency map.

dropout, conv2d_2, max_pooling2d_2, dropout_1. The filter numbers are different for all layers from 16 to 64.

Figure 17. is the output of a saliency map function which is the representation of the importance of each pixel in an image concerning a specific class prediction. The saliency map is computed by taking the gradient of the class score concerning the input image and highlighting the pixels that have the highest absolute gradient values. This means that the pixels with the highest values in the saliency map are the most important for the class prediction, and changing those pixels would have the greatest effect on the prediction.

V. DISCUSSION AND FUTURE SCOPES

The following findings illustrate how the black box model reacts to altered photos, allowing us to infer which characteristics may have been involved. However, this information must still be given to the user understandably. To monitor its

TABLE 14. Our proposed model implications in other medical domains one is for Alzheimer's Disease (AD) and another is for Pneumonia classification from Chest X-ray.

Class	Visualization		
Mild	input image	Grad-CAM	Grad-CAM++
Moderate	input image	Grad-CAM	Grad-CAM++
Non	input image	Grad-CAM	Grad-CAM++
Very mild	input image	Grad-CAM	Grad-CAM++
Normal	input image	Grad-CAM	Grad-CAM++
Pneumonia	input image	Grad-CAM	Grad-CAM++

behaviour, just one trained model was employed, and findings may vary with other model designs and training data sets. Furthermore, the perturbation of input samples comprised only sequential changes.

Our goal was to create a mechanism to deliver domain-specific explanations for a CNN model. While single-sample explanations are useful, knowing the model as a whole is critical. The outcomes of applying our explanation approach to several samples and combining them might be the next stage. There is presently insufficient evidence to relate the observed relevance of feature dimensions to the real score when employing the ABCD rule. Other measures for evaluating explanations should also be explored, providing a possibility for future study.

VI. CONCLUSION

A clinical decision support system's skin image classifier can serve as a second opinion for dermatologists. Although a

large research community has helped, these AI-based systems can only make predictions and cannot explain their rationale. This is where XAI approaches come in. We demonstrated how to approach skin image analysis in a domain-specific manner. For example, if a dermatologist identifies a lesion as a nevus but the model labels it as a melanoma, both the doctor and the patient may wonder “Why?” Our method includes explanations such as “if the color of the lesion is constant, the classifier’s confidence in melanoma diagnosis drops.” The clinician may then notice the color irregularity in the dermatoscopic picture, which is not evident on the lesion, and figure out why the classifier predicted incorrectly. Whether the clinical decision support system supports or opposes the physician’s diagnosis, offering human-readable reasons fosters confidence and improves system knowledge. Furthermore, our perturbation-based explanation technique for diagnosis employing medically relevant and irrelevant characteristics may have implications in other medical domains. In Table 14, we are showing the implications of our model to other medical images dataset. The dataset is just tested by our model. In the future, we will train our model by using attention/transformer so that the interpretability score get increase.

REFERENCES

- [1] S. A. AlSalman, T. M. Alkaff, T. Alzaid, and Y. Binamer, “Nonmelanoma skin cancer in Saudi Arabia: Single center experience,” *Ann. Saudi Med.*, vol. 38, no. 1, pp. 42–45, Jan. 2018.
- [2] K. S. Nehal and C. K. Bichakjian, “Update on keratinocyte carcinomas,” *New England J. Med.*, vol. 379, no. 4, pp. 363–374, Jul. 2018.
- [3] *Key Statistics for Melanoma Skin Cancer*, American Cancer Society, Atlanta, GA, USA, 2022.
- [4] M. A. Albahar, “Skin lesion classification using convolutional neural network with novel regularizer,” *IEEE Access*, vol. 7, pp. 38306–38313, 2019.
- [5] M. R. Hasan, M. I. Fatemi, M. M. Khan, M. Kaur, and A. Zaguia, “Comparative analysis of skin cancer (benign vs. malignant) detection using convolutional neural networks,” *J. Healthcare Eng.*, vol. 2021, Dec. 2021, Art. no. 5895156.
- [6] R. L. Siegel, “Colorectal cancer statistics, 2020,” *CA A, Cancer J. Clinicians*, vol. 70, no. 3, pp. 145–164, 2020.
- [7] S. A. Ajagbe, K. A. Amuda, M. A. Oladipupo, O. F. Afe, and K. I. Okesola, “Multi-classification of Alzheimer disease on magnetic resonance images (MRI) using deep convolutional neural network (DCNN) approaches,” *Int. J. Adv. Comput. Res.*, vol. 11, no. 53, pp. 51–60, Mar. 2021.
- [8] C. Barata, J. S. Marques, and M. E. Celebi, “Deep attention model for the hierarchical diagnosis of skin lesions,” in *Proc. IEEE/CVF Conf. Comput. Vis. Pattern Recognit. Workshops (CVPRW)*, Jun. 2019, pp. 1–9.
- [9] H. P. Soyer, G. Argenziano, V. Ruocco, and S. Chimenti, “Dermoscopy of pigmented skin lesions*(Part II),” *Eur. J. Dermatol.*, vol. 11, no. 5, pp. 483–498, 2001.
- [10] B. Ankad, P. Sakhare, and M. Prabhu, “Dermoscopy of non-melanocytic and pink tumors in Brown skin: A descriptive study,” *Indian J. Dermatopathol. Diagnostic Dermatol.*, vol. 4, no. 2, p. 41, 2017.
- [11] D. Thanh and S. Dvoencko, “A denoising of biomedical images,” *Int. Arch. Photogramm., Remote Sens. Spatial Inf. Sci.*, vol. 40, no. 5, p. 73, 2015.
- [12] M. A. Kassem, K. M. Hosny, and M. M. Fouad, “Skin lesions classification into eight classes for ISIC 2019 using deep convolutional neural network and transfer learning,” *IEEE Access*, vol. 8, pp. 114822–114832, 2020.
- [13] A. H. Shahin, A. Kamal, and M. A. Elattar, “Deep ensemble learning for skin lesion classification from dermatoscopic images,” in *Proc. 9th Cairo Int. Biomed. Eng. Conf. (CIBEC)*, Dec. 2018, pp. 150–153.
- [14] Y. Li and L. Shen, “Skin lesion analysis towards melanoma detection using deep learning network,” *Sensors*, vol. 18, no. 2, p. 556, Feb. 2018.
- [15] J. A. A. Salido and C. Ruiz, “Using deep learning for melanoma detection in dermoscopy images,” *Int. J. Mach. Learn. Comput.*, vol. 8, no. 1, pp. 61–68, Feb. 2018.
- [16] F. Sherif, W. A. Mohamed, and A. Mohra, “Skin lesion analysis toward melanoma detection using deep learning techniques,” *Int. J. Electron. Telecommun.*, vol. 65, no. 4, pp. 597–602, 2019.
- [17] M. R. Hasan, M. I. Fatemi, M. M. Khan, M. Kaur, and A. Zaguia, “Comparative analysis of skin cancer (benign vs. Malignant) detection using convolutional neural networks,” *J. Healthcare Eng.*, 2021.
- [18] M. Z. Ur Rehman, F. Ahmed, S. A. Alsuhibany, S. S. Jamal, M. Z. Ali, and J. Ahmad, “Classification of skin cancer lesions using explainable deep learning,” *Sensors*, vol. 22, no. 18, p. 6915, Sep. 2022.
- [19] W. Gouda, N. U. Sama, G. Al-Waakid, M. Humayun, and N. Z. Jhanjhi, “Detection of skin cancer based on skin lesion images using deep learning,” *Healthcare*, vol. 10, no. 7, p. 1183, Jun. 2022.
- [20] U.-O. Dorj, K.-K. Lee, J.-Y. Choi, and M. Lee, “The skin cancer classification using deep convolutional neural network,” *Multimedia Tools Appl.*, vol. 77, no. 8, pp. 9909–9924, Apr. 2018.
- [21] Y. N. Fu’adah, N. C. Pratiwi, M. A. Pramudito, and N. Ibrahim, “Convolutional neural network (CNN) for automatic skin cancer classification system,” *IOP Conf. Ser., Mater. Sci. Eng.*, vol. 982, no. 1, Dec. 2020, Art. no. 012005.
- [22] C. Barata and J. S. Marques, “Deep learning for skin cancer diagnosis with hierarchical architectures,” in *Proc. IEEE 16th Int. Symp. Biomed. Imag. (ISBI)*, Apr. 2019, pp. 841–845.
- [23] N. Nigar, M. Umar, M. K. Shahzad, S. Islam, and D. Abalo, “A deep learning approach based on explainable artificial intelligence for skin lesion classification,” *IEEE Access*, vol. 10, pp. 113715–113725, 2022.
- [24] A. Ameri, “A deep learning approach to skin cancer detection in dermoscopy images,” *J. Biomed. Phys. Eng.*, vol. 10, no. 6, pp. 801–806, Dec. 2020.
- [25] R. S. Kumar, A. Singh, S. Srinath, N. K. Thomas, and V. Arasu, “Skin cancer detection using deep learning,” in *Proc. Int. Conf. Electron. Renew. Syst. (ICEARS)*, Mar. 2022, pp. 1724–1730.
- [26] F. Stieler, F. Rabe, and B. Bauer, “Towards domain-specific explainable AI: Model interpretation of a skin image classifier using a human approach,” in *Proc. IEEE/CVF Conf. Comput. Vis. Pattern Recognit. Workshops (CVPRW)*, Jun. 2021, pp. 1802–1809.
- [27] L. Wei, K. Ding, and H. Hu, “Automatic skin cancer detection in dermoscopy images based on ensemble lightweight deep learning network,” *IEEE Access*, vol. 8, pp. 99633–99647, 2020.
- [28] O. O. Abayomi-Alli, R. Damaševičius, S. Misra, R. Maskeliunas, and A. Abayomi-Alli, “Malignant skin melanoma detection using image augmentation by oversampling in nonlinear lower-dimensional embedding manifold,” *TURKISH J. Electr. Eng. Comput. Sci.*, vol. 29, no. SI-1, pp. 2600–2614, Oct. 2021.
- [29] S. Maqsood and R. Damaševičius, “Multiclass skin lesion localization and classification using deep learning based features fusion and selection framework for smart healthcare,” *Neural Netw.*, vol. 160, pp. 238–258, Mar. 2023.
- [30] M. Nawaz, T. Nazir, M. Masood, F. Ali, M. A. Khan, U. Tariq, N. Sahar, and R. Damaševičius, “Melanoma segmentation: A framework of improved DenseNet77 and UNET convolutional neural network,” *Int. J. Imag. Syst. Technol.*, vol. 32, no. 6, pp. 2137–2153, Nov. 2022.
- [31] R. R. Selvaraju, M. Cogswell, A. Das, R. Vedantam, D. Parikh, and D. Batra, “Grad-CAM: Visual explanations from deep networks via gradient-based localization,” in *Proc. IEEE Int. Conf. Comput. Vis. (ICCV)*, Oct. 2017, pp. 618–626.
- [32] A. Chattopadhyay, A. Sarkar, P. Howlader, and V. N. Balasubramanian, “Grad-CAM++: Generalized gradient-based visual explanations for deep convolutional networks,” in *Proc. IEEE Winter Conf. Appl. Comput. Vis. (WACV)*, Mar. 2018, pp. 839–847, doi: [10.1109/WACV.2018.00097](https://doi.org/10.1109/WACV.2018.00097).
- [33] K. Mridha, M. I. Islam, S. Ashfaq, M. A. Priyok, and D. Barua, “Deep learning in lung and colon cancer classifications,” in *Proc. Int. Conf. Adv. Comput., Commun. Mater. (ICACCM)*, Nov. 2022, pp. 1–6, doi: [10.1109/ICACCM56405.2022.10009311](https://doi.org/10.1109/ICACCM56405.2022.10009311).
- [34] K. Mridha, S. Kumbhani, S. Jha, D. Joshi, A. Ghosh, and R. N. Shaw, “Deep learning algorithms are used to automatically detection invasive ducal carcinoma in whole slide images,” in *Proc. IEEE 6th Int. Conf. Comput., Commun. Autom. (ICCCA)*, Dec. 2021, pp. 123–129, doi: [10.1109/ICCCA52192.2021.9666302](https://doi.org/10.1109/ICCCA52192.2021.9666302).



KRISHNA MRIDHA (Member, IEEE) was born in Madaripur, Dhaka, Bangladesh, in 1997. He received the bachelor's degree in computer engineering through the Government of India initiative called "Study in India." He is currently a Research Assistant with the Department of Computer Engineering—Artificial Intelligence, Marwadi University, Rajkot, Gujarat, India. From 2017 to 2018, he was a Junior Instructor in information and communication technology with the Private Medical Technology Institute, Dhaka. In 2019, he came to India to pursue his bachelor's degree. In his bachelor's journey, he published some research articles related to medical diagnosis. He won the IEEE Student Beset Student Research Paper Award, in 2021.



SUSAN KHADKA is currently pursuing the Bachelor of Technology degree in computer engineering through a scholarship provided by "Study in India," an initiative by the Government of India. His research interests include AI, ML algorithms, deep learning algorithms, and models.



MD. MEZBAH UDDIN was born in Cumilla, Bangladesh. He is currently pursuing the bachelor's degree in computer engineering in India through the study in India Scholarship, which is sponsored by the Indian Government. His future goal is to pursue the Ph.D. degree in healthcare AI and continue to contribute to the development and implementation of AI solutions in the healthcare industry. His research interest includes the field of artificial intelligence in healthcare.



JUNGPIL SHIN (Senior Member, IEEE) received the B.Sc. degree in computer science and statistics and the M.Sc. degree in computer science from Pusan National University, South Korea, in 1990 and 1994, respectively, and the Ph.D. degree in computer science and communication engineering from Kyushu University, Japan, in 1999, under a scholarship from the Japanese Government (MEXT). He was an Associate Professor, a Senior Associate Professor, and a Full Professor with the School of Computer Science and Engineering, The University of Aizu, Japan, in 1999, 2004, and 2019, respectively. He has coauthored more than 300 published papers for widely cited journals and conferences. His research interests include pattern recognition, image processing, computer vision, machine learning, human-computer interaction, non-touch interfaces, human gesture recognition, automatic control, Parkinson's disease diagnosis, ADHD diagnosis, user authentication, machine intelligence, handwriting analysis, recognition, and synthesis. He is a member of ACM, IEICE, IPSJ, KISS, and KIPS. He served as the program chair and as a program committee member for numerous international conferences. He serves as an Editor for IEEE journals and for *Sensors* (MDPI) and *Electronics*. He serves as a reviewer for several major IEEE and SCI journals.



M. F. MRIDHA (Senior Member, IEEE) received the Ph.D. degree in AI/ML from Jahangirnagar University, in 2017. He is currently an Associate Professor with the Department of Computer Science, American International University-Bangladesh (AIUB). Before that, he was an Associate Professor and the Chairman of the Department of CSE, Bangladesh University of Business and Technology. He was also a CSE Department Faculty Member with the University of Asia-Pacific and as the Graduate Head, from 2012 to 2019. His research experience, within both academia and industry, results in over 120 journals and conference publications. His research work contributed to the reputed *Scientific Reports*, *Nature*, *Knowledge-Based Systems*, *Artificial Intelligence Review*, IEEE ACCESS, *Sensors*, *Cancers*, and *Applied Sciences*. His research interests include artificial intelligence (AI), machine learning, deep learning, natural language processing (NLP), and big data analysis. For more than ten years, he has been with the master's and undergraduate students as a supervisor of their thesis work. He has served as a program committee member in several international conferences/workshops. He served as an Associate Editor for several journals, including *PLOS One* journal. He has served as a reviewer of reputed journals and IEEE conferences, such as HONET, ICIEV, ICCIT, IJCCI, ICAEE, ICCAIE, ICSIPA, SCORED, ISIEA, APACE, ICOS, ISCAIE, BEIAC, ISWTA, IC3e, ISWTA, CoAST, icIVPR, ICSCT, 3ICT, and DATA21.